



# **(A)ATSR Exploitation Plan Volume 5**

## **Review of Remotely Sensed Land Surface Temperature (LST) Products and their Applications**

Written by: The (A)ATSR Science Team

Edited by: Hugh Kelliher (Space ConneXions Limited)

Checked by: John Remedios (University of Leicester)

Approved by:

David Llewellyn-Jones  
*AATSR Principal Investigator*

Wolfgang Lengert  
*On behalf of ESA*



## Table of Contents

<b>1</b>	<b>Introduction.....</b>	<b>3</b>
<b>2</b>	<b>Satellite observations of LST .....</b>	<b>5</b>
2.1	Theoretical basis for the remote sensing of LST .....	5
2.2	The (A)ATSR LST product .....	6
2.3	Other LST products .....	7
<b>3</b>	<b>The applications of LST products .....</b>	<b>9</b>
3.1	LST and urban climate change.....	9
3.2	Detection of land cover changes using LST products.....	12
3.3	LST and soil moisture retrieval .....	14
3.4	Fire detection and burned area mapping.....	17
3.5	Volcanic activity and earthquakes .....	21
3.6	Forest mapping.....	22
3.7	Energy balance (sensible/latent heat and evaporation).....	22
3.8	Connection between convection and LST .....	23
3.9	Connection between gas emissions and LST.....	24
3.10	Other applications .....	27
3.11	Model predicted LST .....	28
<b>4</b>	<b>Possible exploitation of AATSR LST applications.....</b>	<b>29</b>
<b>5</b>	<b>References .....</b>	<b>31</b>
	<b>Appendix A: List of acronyms.....</b>	<b>36</b>

## 1 INTRODUCTION

Land surface temperature (LST) is a key boundary condition in many remote sensing-based land surface modelling schemes (Kustas and Norman, 1996). LST is important because it determines the effective radiating temperature of the Earth's surface. This controls the surface air temperature as well as the clear sky outgoing long-wave radiation, which is important in the energy balance of the Earth. It is also a major factor in determining the partition of the available energy into sensible and latent heat fluxes. For example, the rate of change of LST is sensitive to the characteristics of the land surface such as soil moisture, land use and vegetation. Regions of high soil moisture content or dense vegetation that have access to a source of moisture exhibit cooler LST than dry soil or vegetation that is stressed because of a lack of available soil moisture (Gillies et al., 1997; Verstracten et al., 2006).

Land surface changes provide important feedbacks, as anthropogenic climate changes (e.g., increased temperature, changes in precipitation, changes in net radiative heating, and the direct effects of CO<sub>2</sub> and other gases, such as water vapour) influence the state of the land surface (e.g., soil moisture, albedo, roughness and vegetation; climate change, 2001). Exchanges of energy, momentum, water, heat and carbon between the land surface and the atmosphere can be defined in models as functions of the type and density of the local vegetation and the depth and physical properties of the soil. Changes in land-surface cover (e.g., urbanization, deforestation and desertification) can affect global climate in several ways. For example, large-scale deforestation in the humid tropics (e.g., South America, Africa and Southeast Asia) has been identified as the most important ongoing land-surface process because it reduces evaporation and increases surface temperature (Meyer, 1996; Betts, 2001).

Land-surface databases have been improved using satellite observations. Previous research has already shown that the LST products retrieved from the satellite imagery can be used to detect the land surface changes, such as urbanization, deforestation and desertification, that can significantly improve our ability to monitor land-surface changes in a consistent manner. Currently available satellite thermal infrared sensors (e.g., (A)ATSR, AVHRR, MODIS, Landsat TM and geostationary sensors) provide different spatial resolution and temporal coverage data that can be used to estimate land surface temperature. The thermal emission property of a material is representative of the upper several centimetres of the surface. Since in thermal remote sensing we measure the emitted radiation, it proves to be complementary to other remote sensing data (e.g., visible, near-infrared and microwave) and even unique in contributing the identification of surface materials and features such as geothermal anomalies, rock types, soil moisture etc. (Prakash. 2000).



A new AATSR LST data product has been available since March 2004. This product provides global observation of LST, derived from split-window radiances, at 1km spatial resolution, with a target accuracy of 2.5K during the day and 1K at night. However, as it is relatively new, very few applications have used this product in practise. This volume of the (A)ATSR Exploitation Plan (AEP) reviews the current remotely sensed LST products (including (A)ATSR, AVHRR and MODIS) and their applications, after which the exploitation of (A)ATSR LST is discussed.

## 2 SATELLITE OBSERVATIONS OF LST

### 2.1 Theoretical basis for the remote sensing of LST

The extensive need for land surface temperature (LST) data for environmental studies and management of the Earth's resources has made the remote sensing of LST an important academic topic during the last two decades. LST is generally defined as the skin temperature of the ground (Qin and Karnieli, 1999). For the bare soil surface, LST is the soil surface temperature. However, the ground is far from a skin or homogeneous surface. This makes the understanding of LST from surfaces such as vegetated ground, difficult. The remote sensing of LST is based on the thermal spectral (long wave) radiation from the ground. Thus, LST of dense vegetated ground can be viewed as the canopy surface temperature of the vegetation, and in sparse vegetated ground, it is the average temperature of the vegetation canopy, vegetation body and the soil surface under the vegetation. Usually, LST changes in an obvious way in a small distance such as 1m (Ottle and Vidal-Madjar, 1992). However, the spatial resolution of most remote sensing data for LST is low compared with the difference of LST on the ground. Thus, LST in remote sensing means the average surface temperature of the ground under the pixel scale mixed with different fractions of surface types (Kerr et al., 1992).

The theoretical basis for the remote sensing of LST is that the total radiative energy emitted by the ground surface increases rapidly with increase in temperature. The spectral distribution of the energy emitted by a ground object also varies with temperature. According to Wien's Displacement Law on the relationship between spectral radiance and wavelength, for the Earth, with an ambient temperature of 300K, the peak of its spectral radiance occurs at about 9.6 $\mu$ m (Lillesand and Kiefer, 1987). Therefore, theoretically, the thermal energy in relation to the physical temperature of the ground surface can be remotely observed by using sensors operating at wavelengths around 10  $\mu$ m, which have been defined as thermal channels in remote sensing systems.

On the other hand, the spectral characteristics of the atmosphere indicate that there is an atmospheric window in the spectral region 8-13  $\mu$ m, where atmospheric absorption is minimum and through which the energy from the ground surface can transmit to space without great losses. Despite having relatively high atmospheric transmission, atmospheric attenuation is still significant in these 'window' channels. Most of the attenuation at these wavelengths is due to water vapour absorption, and is also affected by atmospheric temperature, aerosols etc. To overcome the problem of an unknown atmosphere, the multi-channel approach, called 'split-window' (Prata and Cechet, 1999; Qin and Karnieli, 1999), has been developed to retrieve LST using measurements from at least two different spectral channels (at approximately 11  $\mu$ m and 12  $\mu$ m).



## 2.2 The (A)ATSR LST product

(A)ATSR is primarily designed to measure global Sea Surface Temperature (SST). However, an LST product has been available since March 2004 due to the increasing need for it in climate research. This product provides global observations of LST, derived from split-window radiances, at 1km spatial resolution, with a target accuracy of 2.5K during the day, and 1K at night. (A)ATSR makes spectral radiance measurements in both the longwave and shortwave infrared (Table 2-1). The surface temperature was derived using 11µm and 12 µm channels. A nadir-only split-window algorithm is utilised, where

$$LST = a f, i, pw + b f, i (T_{11} - T_{12}) + n + (b f, i + c f, i) T_{12}, \tag{1}$$

where a, b and c are coefficients that depend on land cover class (or biome) (i), fractional vegetation cover (f) and precipitable water (pw), and T11 and T12 are the AATSR brightness temperatures (BT) in the 11µm and 12µm channels, respectively. There are currently 13 land cover classes and one lake class. The auxiliary land cover class, fractional vegetation and precipitable water data are tabulated on 0.5° grids, where f and pw are also dependent on the season and time of day, although the latter is currently only in effect for one biome (lake class). The algorithm also has some dependence on satellite viewing angle (θ) within the variables n and a as the AATSR nadir view deviates from true nadir towards the edges of the swath (Noyes, 2006).

<i>Channel µm</i>	<i>Central wavelength µm</i>	<i>Bandwidth µm</i>	<i>Primary Application</i>
0.55	0.555	0.02	Chlorophyll
0.66	0.659	0.02	Vegetation index
0.87	0.865	0.02	Vegetation index
1.6	1.61	0.30	Cloud clearing
3.7	3.70	0.30	Sea surface temperature
11	10.85	1.00	Sea surface temperature
<b>12</b>	12.00	1.00	Sea surface temperature

**Table 2-1: (A)ATSR spectral channels (Llewellyn-Jones et al., 2001; Noyes, 2006)**



The detailed product algorithm based on the radiative transfer equation has been described by Prata (2000) and some studies have proved the product has reasonable accuracy. However, how to turn this product into a scientific or operational application needs further investigation.

## 2.3 Other LST products

In addition to the (A)ATSR LST product, there are several operational LST products from other sensors. Examples include the Advanced Very High Resolution Radiometers (AVHRR) on board NOAA's polar orbiting satellites, the MODerate Resolution Imaging Spectroradiometers (MODIS) on board the Terra and Aqua polar-orbiting satellites, and the Spinning Enhanced Infrared and Visible Imager (SEVIRI) on-board geostationary Meteosat-8. Other sensors, such as passive microwave radiometers also can provide the brightness temperature, which has advantage of cloud penetration, but lower radiometric accuracy comparing with thermal infrared sensors. Li et al. (2004) derived LST from Landsat 5 and 7 during SMEX02/SMACEX field campaign, which has high spatial resolution (120m for Landsat-5 and 60m for Landsat-7, respectively), however, with low temporal resolution (16 days). The last two sensors may be useful for specific purposes, but they are not discussed any further since they are not being used widely.

The land surface skin temperature diurnal cycle is an important element of the climate system (Aires, et al., 2004; Jin and Dickinson 1999). This variable, however, cannot be directly obtained globally from polar orbiting satellites because such satellites only pass a given area twice per day or less and because their infrared channels cannot observe the surface when the sky is cloudy. Due to the strong and variable diurnal cycle of LST, measurements separated by days or even hours are of more limited use. Geostationary sensors (e.g., SEVIRI) can capture the diurnal cycle of LST due to high temporal resolutions, however some disadvantages limit their applications (see Table1). Data from polar-orbiting sensors, such as the AATSR, have the potential to resolve this problem and some researchers are currently investigating combining LSTs from polar-orbiting and geostationary satellites in order to generate a high-spatial resolution, high-temporal resolution LST data set (Noyes, 2006; Reutter et al., 1996). Alternatively, to obtain the skin temperature diurnal cycle and fully utilize satellite measurements, Jin and Dickinson (1999) designed an efficient algorithm that combines model results with satellite and surface-based observations and interpolates satellite twice-daily observations into the diurnal cycle.

A good review of each sensor including its strengths and limitations has been documented in the literature (Noyes, 2006), thus only a summary is given in Table 2-2.

Sensor	Resolution	Advantages and Disadvantages
AATSR	1km, ~3days revisit time	The product has good radiometric accuracy (<0.1K), on board calibration, with a target accuracy of 2.5K during the day, and 1K at night (Llewellyn-Jones et al., 2001; Noyes, 2006). It has a forward and nadir dual-view for a single point, which is useful when combining the LST product with geostationary sensors. The 3 days revisit time might be a limiting factor, because it cannot catch either the diurnal cycle or daily temperature difference (maximum – minimum).
AVHRR	1km, Two satellites Twice per day	Day-time overpasses occur during the period of maximum surface/air temperature (~ 13:00 to 14:00 local time) and night-time overpasses occur during the period of minimum surface/air temperature (~ 02:00 to 03:00 local time). It can capture the daily temperature difference (LST <sub>day</sub> – LST <sub>night</sub> ), which can be representative of the surface properties, thermal inertia and moisture content etc. This dataset has a relatively long data record (more than 20 years) and currently is widely used in many applications.
MODIS	1km, Terra and Aqua Twice per day  Terra: 10:30am/pm local time Aqua: 1:30am/pm local time	MODIS, with its 2330km viewing swath width flying onboard Terra and Aqua, provides almost complete global coverage in one day. It acquires data in 36 high spectral resolution bands between 0.415 and 14.235 μm with spatial resolution of 250m (2 bands), 500m (5 bands), and 1000m (29 bands). MODIS LST is derived from the corrected two thermal bands (bands 31 and 32 in the 10.5-12.5 μm spectra) using a view-angle-dependent split-window LST algorithm for MODIS with reported accuracy of better than 1K (Savtchenko et al., 2004; Wan, 1999). MODIS LST can also capture the daily temperature difference (LST <sub>day</sub> – LST <sub>night</sub> ).
SEVIRI	3-5km, 15mins	SEVIRI is a new geostationary sensor. It has a higher temporal frequency, which can capture the diurnal cycle of LST. However, LST retrieval from geostationary satellites is more challenging due to the higher zenith angles, and therefore increased atmospheric attenuation, at high latitudes. Due to the larger pixel size of geostationary sensors, these observations of LST are more difficult to validate against <i>in situ</i> data. The pixel size also limits the use of geostationary LST data for some applications.

**Table 2-2: A summary of current remotely sensed LST products**

### 3 THE APPLICATIONS OF LST PRODUCTS

Due to the fact that AATSR LST is a relatively new product, few studies are available for review. This section therefore reviews the applications of other LST products (e.g., AVHRR, MODIS and SEVIRI). The possibility of similar applications with the AATSR LST product will be discussed in Section 4.

#### 3.1 LST and urban climate change

The surface temperature is of prime importance to the study of urban climate, not only in obtaining boundary conditions of the atmosphere, but also in understanding the environmental conditions necessary to sustain human beings. Urbanization, including residential, commercial and industrial developments, creates one of the most dramatic human-induced changes on a natural ecosystem, causing the local air and surface temperature to rise several degrees higher than the temperatures of the surrounding rural areas (Figure 3-1). The interactions of urban surfaces with the atmosphere are governed by surface heat fluxes, the distribution of which is drastically modified by urbanization. The main contributing factors are changes in the physical characteristics of the surface (albedo, thermal capacity, heat conductivity), owing to the replacement of vegetation by asphalt and concrete; the decrease of surface moisture available for evapotranspiration; changes in the radiative fluxes and in the near surface flow, owing to the complicated geometry of streets and tall buildings, and anthropogenic heat (Dousset and Gourmelon, 2003).

Previous studies have demonstrated that the LST product retrieved from TIR (thermal infrared) sensors can be used to monitor the urban heat island (UHI) effect. For example, Pongracz et al. (2006) used day- and night-time surface temperature time series observed by MODIS to determine UHI intensities over the ten most populated cities of Hungary. Spatial structures of UHIs were determined and compared for different seasons and macrocirculation conditions. Hung et al. (2006) analyzed the UHI in 18 Asian mega cities using cloud free, day- and night Terra MODIS LST products acquired between 2001 and 2003. Spatial pattern of UHIs for each city were examined over its diurnal cycle and seasonal variations. They found that both the magnitude and extent of UHIs were highly positively correlated to population size of the cities, indicating the significant impacts of urban growth on the UHI problems in Asia.

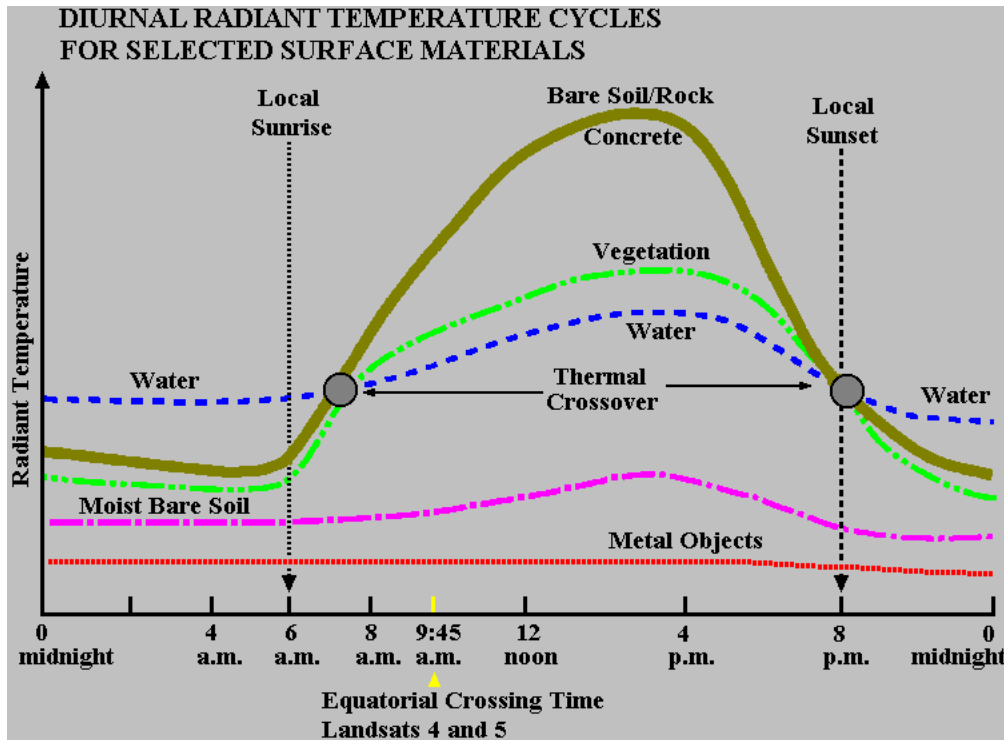
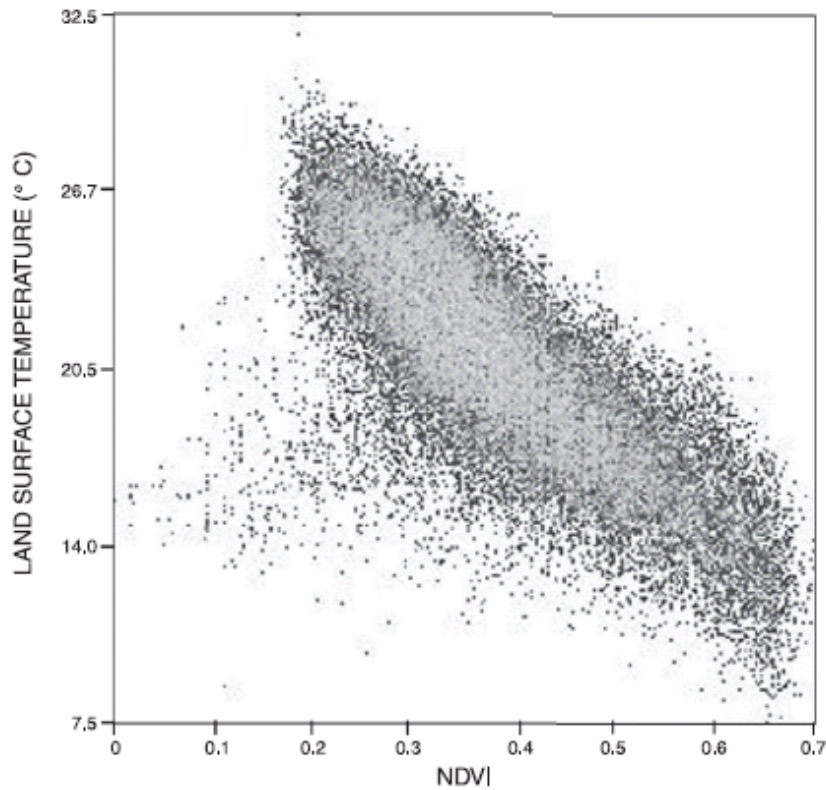


Figure 3-1: Diurnal radiant temperature cycles for selected surface materials

([http://employees.oneonta.edu/baumanpr/geosat2/Urban\\_Heat\\_Island/Urban\\_Heat\\_Island.htm](http://employees.oneonta.edu/baumanpr/geosat2/Urban_Heat_Island/Urban_Heat_Island.htm))

Research on urban surface energy balances using thermal data coupled with climate models (e.g., Carlson and Arthur, 2000; Owen et al., 1998) showed that the partitioning of sensible and latent heat fluxes and thus, surface radiant temperature response, is a function of varying surface soil water content and vegetation cover. Using NOAA AVHRR data, Gallo et al. (1993) pinpointed the significance of vegetation index as an important indicator of urban-rural differences in minimum air temperature for 37 US cities. Dousset and Gourmelon (2003) analyzed spatial and temporal variations of urban LSTs and land cover using combined AVHRR LST and SPOT-HRV Normalized Difference Vegetation Index (NDVI) data. The study was based on summertime microclimate analyses of the Los Angeles and Paris metropolises. They found that effects of urban surface properties, such as built-up area, vegetation and water on the surface temperature were significant. Their results show (i) the effect of surface physical properties, especially in downtown business and industrial districts that display heat-islands larger than 7°C; (ii) The coolest areas were the urban parks in the vicinity of the Seine river, which indicates water (river and lake in the city) has a cooling influence on surface temperature; (iii) the negative correlation between afternoon LST and normalized vegetation index (Figure 3-2), which confirms the cooling effect of urban parks; (iv) the correlation between variations of surface temperature and ozone concentration at diurnal and longer time scales (Figure 3-3).



**Figure 3-2: Bivariate histogram of the diurnal LST amplitude (LST<sub>day</sub> – LST<sub>night</sub>) of the Paris basin between the images acquired on August 7 at 13:28 UTC and on August 8 at 03:27 UTC, versus the NDVI (Dousset and Gourmelon,2003).**

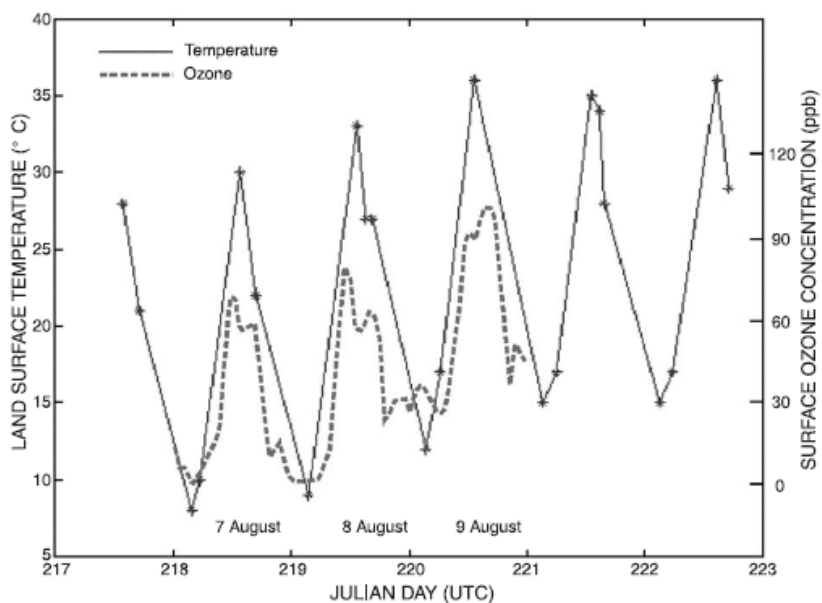


**Figure 3-3: Diurnal cycle of the median LST of the Paris basin from 22 NOAA-AVHRR thermal IR images, August 5 – 10, 1998; and collocated surface ozone concentration from the ESQUIF experiment, August 7 – 9, 1998 (Dousset and Gourmelon, 2003).**

### 3.2 Detection of land cover changes using LST products

Sobrino and Raissouni (2000) demonstrated that LST and NDVI retrieved from NOAA AVHRR data could be used to monitor desertification. They used two methods to analyse the spatial-temporal dynamics of LST and NDVI (10-day composites afternoon images) in Morocco:

- (1) the method of the area of the triangle (MAT), based on a description of the evolution of the NDVI and LST over an annual period;
- (2) the method of the slope, which analyses the slope of the line defined by the months of the maximum NDVI and the minimum LST.

Results from both methods show that the desertification area corresponds with low NDVI and high LST. Table 3-1 describes the research sites and Figure 3-4 and Figure 3-5 show the relationship between the LST and NDVI. Lambin and Ehrlich (1997) also applied a change index based on remotely sensed surface temperature and vegetation indices (Ts/NDVI) to study land-cover changes from 1982-1991 at a continental scale. The results of their study demonstrate that interannual land cover changes in Africa mostly involve erratic variations in land-cover conditions due to interannual climatic variability and temporary modifications in seasonality.

<i>Colour</i>	<i>NDVI</i>	<i>Characteristics</i>	<i>Name</i>
Blue	<0.05	Deserts. Limited opportunities for the development of the human activities	Zone 1
Cyan	0.05-0.10	Dry lands. Low precipitation, high temperatures, low level of water retention	Zone 2
Sea Green	0.10-0.15	Low precipitation. Able to sustain the vegetation	Zone 3
Green	0.15-0.20	Similar to Zone 3	Zone 4
Yellow	0.20-0.25	Medium precipitation. Area of vegetation	Zone 5
Red	0.25-0.30	Areas of abundant vegetation. High precipitation	Zone 6
<b>Black</b>	>0.30	Higher mountains	Zone 7

**Table 3-1: Zones of the study area and their main characteristics (Sobrino and Raissouni, 2000)**

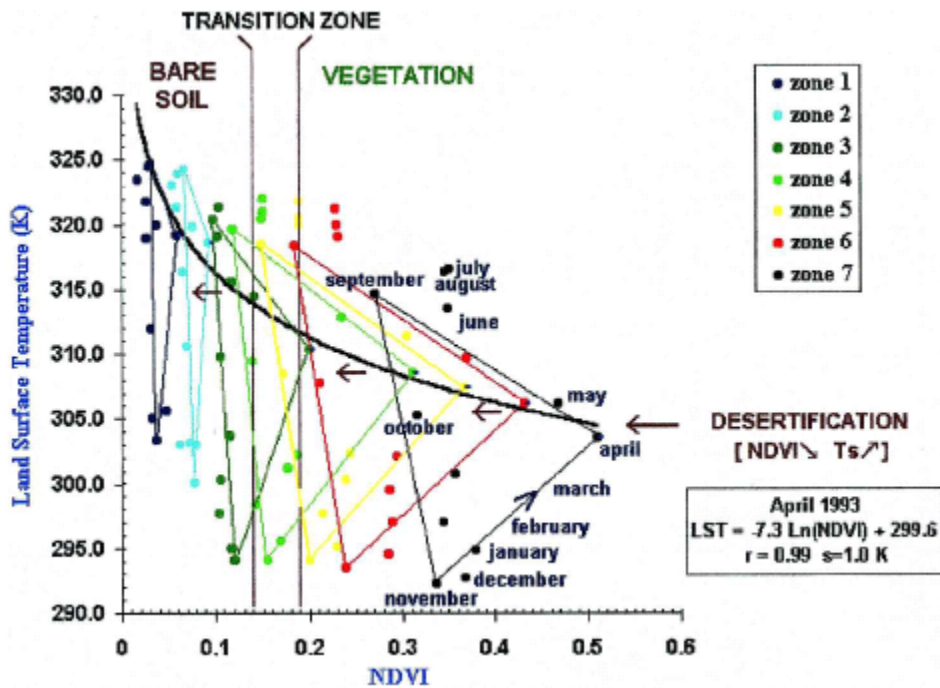


Figure 3-4: Analysis of the area of the triangle LSTmin/NDVImax (LST in K and NDVI %). (Sobrino and Raissouni, 2000).

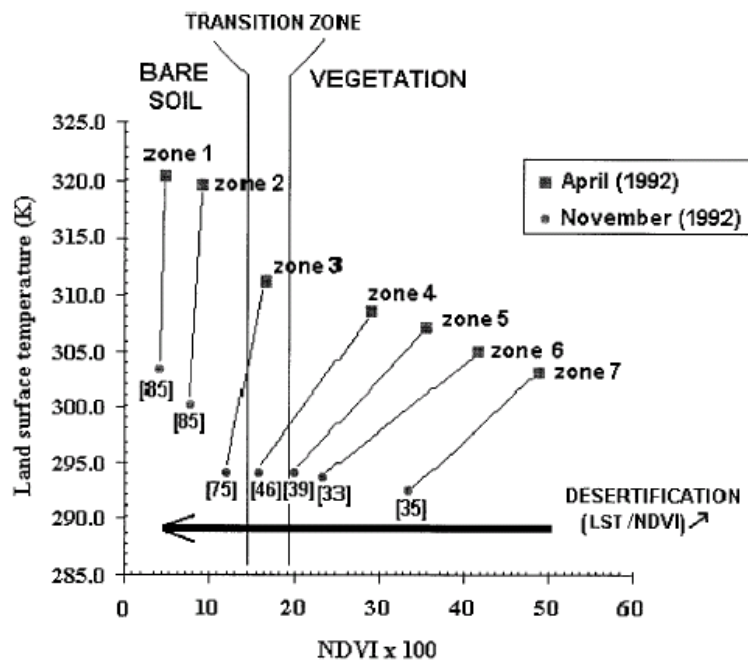


Figure 3-5: Analysis of the slope LSTmin/NDVImax (LST in K and NDVI %). The values in square brackets represent the arctangent value of the slope (Sobrino and Raissouni, 2000).

### 3.3 LST and soil moisture retrieval

LST differences ( $\Delta LST$ ) and albedo are used in the definition of thermal inertia (TI), to assess the space–time variability of soil moisture content (SMC) for the purpose of water balance model calibration, water limitation of photosynthesis, etc. TI is a body property of materials, which describes their resistance to temperature variations. Its mathematical formulation is:

$$TI = \sqrt{\rho \cdot K \cdot c} \quad (2)$$

In Equation (2):

<i>TI</i>	<i>is the thermal inertia [<math>J m^{-2} K^{-1} s^{-1/2}</math>];</i>
$\rho$	is the material density [ $kg m^{-3}$ ];
<i>K</i>	is the thermal conductivity [ $W m^{-1} K^{-1}$ ];
<i>c</i>	is the specific heat [ $J kg^{-1} K^{-1}$ ].

Water bodies have a higher TI than dry soils and rocks, and exhibit a lower diurnal temperature fluctuation. When soil water content increases, TI increases proportionately as well, thereby reducing the diurnal temperature fluctuation range. TI can be derived from the temperature diffusion equation. A much simpler formulation of TI is the apparent thermal inertia (ATI) which is derived directly from multi-spectral remote sensing imagery. Mitra and Majumdar (2004) inferred ATI using satellite-based spectral surface albedo  $\alpha_0$  and the diurnal temperature range  $\Delta LST_0$ :

$$ATI = C \frac{1-\alpha_0}{\Delta LST} \quad (3)$$

wherein

$$\Delta LST_0 = LST_{0,d} - LST_{0,n} \quad (4)$$

and

$$C = \sin \theta \sin \varphi (1 - \tan^2 \theta \tan^2 \varphi) + \cos \theta \cos \varphi \arccos(-\tan \theta \tan \varphi) \quad (5)$$

In Equations (3), (4) and (5):

$ATI$	is the apparent thermal inertia [ $K^{-1}$ ];
$C$	is the solar correction factor [-];
$\theta$	is the latitude [-];
$\varphi$	is the solar declination [-];
$\alpha_0$	is the broadband albedo [-];
$LST_{0,d}$	is the brightness temperature in the early afternoon [K];
$LST_{0,n}$	is the brightness temperature after midnight [K];
$\Delta LST_0$	is the difference between the afternoon and midnight brightness temperature [K];

ATI represents the temporal and spatial variability of soil and canopy moisture (Tramutoli et al., 2000). The higher ATI is, the higher the moisture content of the surface. Therefore, the Soil Moisture Saturation Index  $SMSI_0$  can be derived from the thermal infrared satellite data:

$$SMSI_0(t) = \frac{ATI(t) - ATI_{min}}{ATI_{max} - ATI_{min}} \quad (6)$$

where  $ATI(t)$  is the apparent thermal inertia [ $K^{-1}$ ] at time  $t$ ;  $ATI_{min}$  is the minimum apparent thermal inertia [ $K^{-1}$ ];  $ATI_{max}$  is the maximum apparent thermal inertia [ $K^{-1}$ ].

The soil moisture content (SMC) can be derived from:

$$\theta(t) = SMSI_0(t)(\theta_{sat} - \theta_{res}) + \theta_{res} \quad (7)$$

where  $\theta(t)$  is volumetric soil moisture content at a time  $t$ ;

$\theta_{sat}$ , is volumetric saturated soil moisture content;

$\theta_{res}$  is volumetric residual soil moisture content.

Based on equations 2 to 7, Verstraeten et al. (2006) presented a method to estimate SMC from optical and thermal spectral information from METEOSAT imagery, based on thermal inertia (see Figure 3-6). Minimum and maximum TI values from time series satellite imagery are combined in the SMSI. To convert surface to soil profile values, a Markov type filter is used, based on a simple two layer water balance equation (the surface layer and the reservoir

below) and an autocorrelation function. Ten-daily SMC values are compared with up-scaled (using AVHRR/NDVI) observations on 10 EUROFLUX sites in Europe for the 1997 growing season (March–October). Validation shows soil moisture retrieval using this method has a reasonable accuracy.

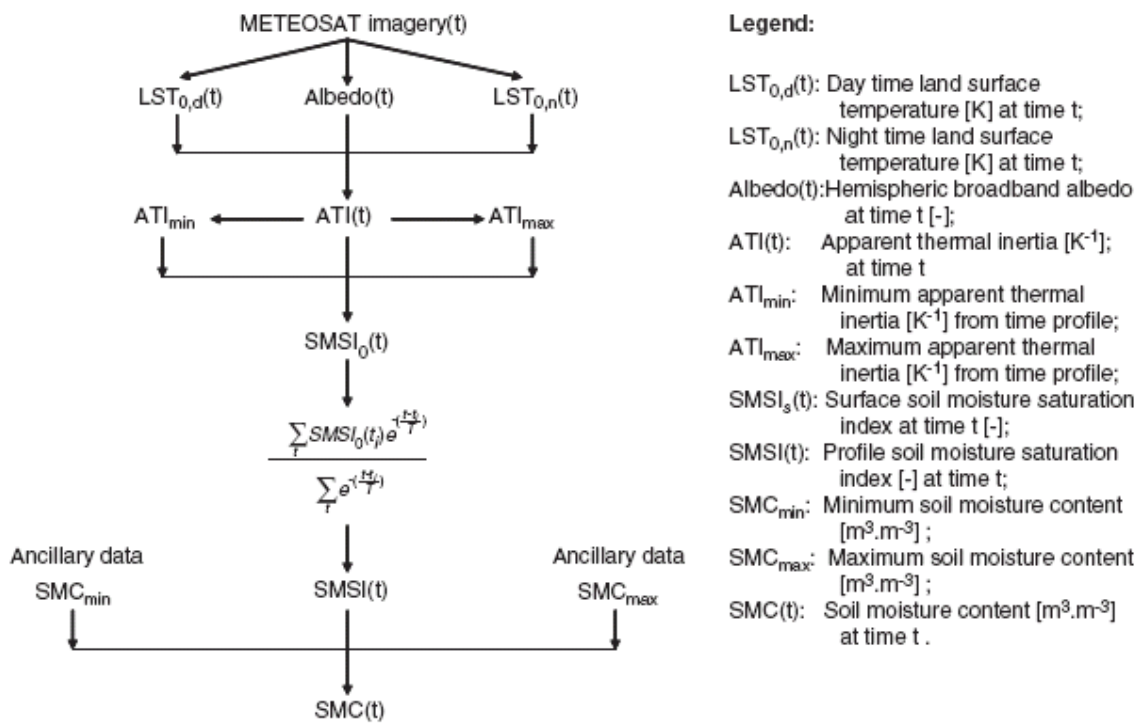


**Figure 3-6: Flow chart with the different steps required for the retrieval of SMC from visible and thermal METEOSAT imagery and ancillary data. The symbols are explained in the legend.**

Gillies et al. (1997) have produced an inversion procedure to estimate surface soil water content as surface moisture availability ( $M_0$ ), NDVI, fractional vegetation cover ( $F_r$ ) and the instantaneous surface energy fluxes (Surface Radiant Temperature, °C), using remote multispectral measurements made from an aircraft. Figure 3-7 shows the relationship between these variables.

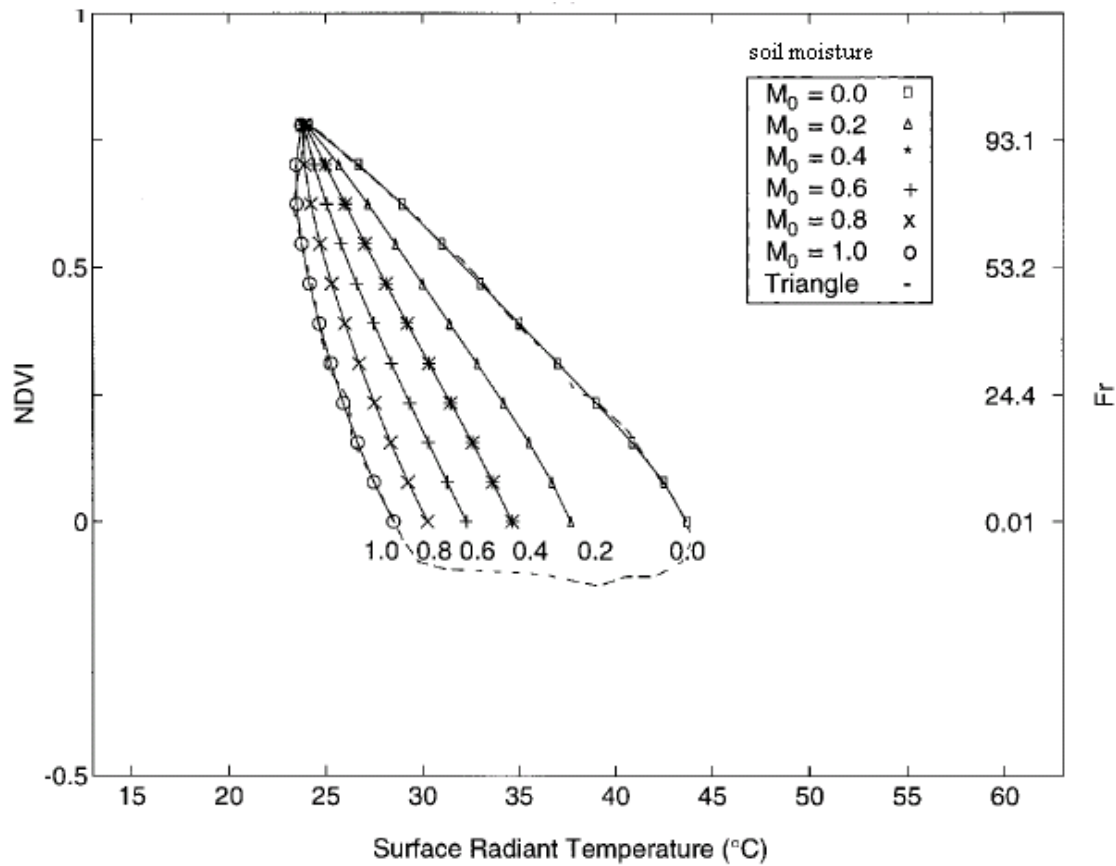


**Figure 3-7: The relationship between surface temperature, NDVI and moisture content (Gillies et al., 1997). Data from MONSOON'90 at Walnut Gulch, 9 August 1990.**

### 3.4 Fire detection and burned area mapping

The emissions from burning biomass contribute significantly to the quantities of CO<sub>2</sub> and trace gases in the atmosphere that are of major importance for both environmental and global climate change. For instance, biomass burning contributes up to 40%, 16% and 43% of the total emissions of anthropogenic origin for carbon dioxide (CO<sub>2</sub>), methane (CH<sub>4</sub>) and carbon monoxide (CO), respectively (Houghton et al., 1995). Fire also plays an important role in land cover change processes such as deforestation, and thus it is important to monitor the land surface that is burned on both regional and global scales.

The ATSR-2, AVHRR and MODIS LST data have been widely used for burned land mapping and previous studies have shown accurate performances in regional-to-global coverage (Simon et al., 2004; Barbosa et al., 1999; Fraser et al., 2000). The principle of this application is based on charcoal and ash absorbing more energy than vegetation, especially in the NIR. This effect, plus the removal of vegetation shading and alteration of soil water relationships means that burned areas tend to have higher temperatures than surrounding non-affected vegetation, at least in the short-term after fire. In addition, charcoal and charred fuels

deposited over the ground after a fire have very low reflectance in the visible and near infrared bands. Therefore, a recent burned scar tends to the minimum value of a time series (Cabral et al., 2003; Sousa et al., 2003).

Barbosa et al. (1999) presented a methodology to detect burned surfaces using a long-time series of low resolution NOAA AVHRR Global Area Coverage (GAC) 5km data, applied at a continental scale over Africa. The burnt area indices that were derived were based on a multi-temporal multi-threshold and the spectral changes of the land surface after an occurrence of fire. By using different sets of AVHRR channels and derived indices, spectral signatures have been determined for burned and unburned surfaces. Indices that make use of the information contained in Channel 2 (0.735-1 $\mu$ m) and Channel 3 (1.58-3.93  $\mu$ m) are the best for detecting burned areas. The results showed excellent agreement at the continental scale with known temporal and spatial patterns of active fires. Validation of the algorithm by comparison with a number of Landsat TM images showed an overall accuracy of 71%.

Chuvieco et al. (2005) used several criteria to generate multitemporal composites of daily AVHRR and MODIS images for burned land mapping and tested them using data acquired over the Iberian Peninsula in 2001, 2003 and 2004. Seven different compositing techniques were tested, based on maximizing NDVI and brightness/surface temperature, and minimizing reflectance and sensor zenith angles. Their results show that the composite criteria provides the most accurate images for burned land mapping based on maximizing brightness/surface temperatures, either as the only factor or in conjunction with minimizing sensor zenith angle or near infrared (NIR) reflectance.

Another fire detection application is to estimate the dead fuel moisture content (FMC), which is useful to better manage fire suppression resources and to reduce accidental fire ignitions and mitigate fire propagation rates (Chuvieco et al., 2004). FMC is defined as the percentage of water weight ( $W_w$ ) over sample dry weight ( $W_d$ ):

$$FMC = \left( \frac{W_w - W_d}{W_d} \right) \times 100 \quad (8)$$

The moisture content of fuel is a critical parameter in fire ignition because flammability is closely dependent on it (Dimitrakopoulos and Papaioannou, 2001). Commonly, the estimation of FMC is based on meteorological danger indices, which attempt to account for the adsorption-evaporation relationships in inert materials (Simard, 1968). However, meteorological data are frequently not available for fire-prone areas, which requires the application of spatial interpolation techniques that may introduce additional errors (Chuvieco et al., 2004).

Within the context of fire danger estimation, good correlations between live FMC and multitemporal series of NOAA AVHRR data have been found for herbaceous species using NDVI data (Chladil and Nunez, 1995; Paltridge and Barber, 1988), but problems were found for shrubs and trees (Chuvienco et al., 1999). Additionally, plant canopy temperature is affected by FMC changes because water availability is a critical parameter in plant evapotranspiration. Some recent studies have demonstrated that the combined use of surface temperature and NDVI show statistically stronger relationships with water content than either of the two variables alone (Chuvienco et al., 2004; Chuvienco et al., 2005; Manzo-Delgado et al., 2005). For example, Chuvienco et al. (2004) presented an empirical method for deriving FMC for Mediterranean grasslands and shrub species based on multitemporal analysis of NOAA AVHRR data. The empirical function was derived from a 4-year series and includes multitemporal composites of AVHRR's NDVI and surface temperature (ST) values, as well as a function of the day of the year. It was tested using data from 2 other years on the same site as well as other sites with similar species, but very distant from each other and with different elevation ranges. The results show that the model provides a consistent estimation of FMC, with high accuracies for all study sites and species considered. Figure 3-8 shows a scatterplot of NDVI against ST for different FMC values observed in the Cabaeros site from Chuvienco et al., 2004, which shows a trend towards low values of FMC when low values of NDVI and high ST values occur, both for grasslands and shrublands.

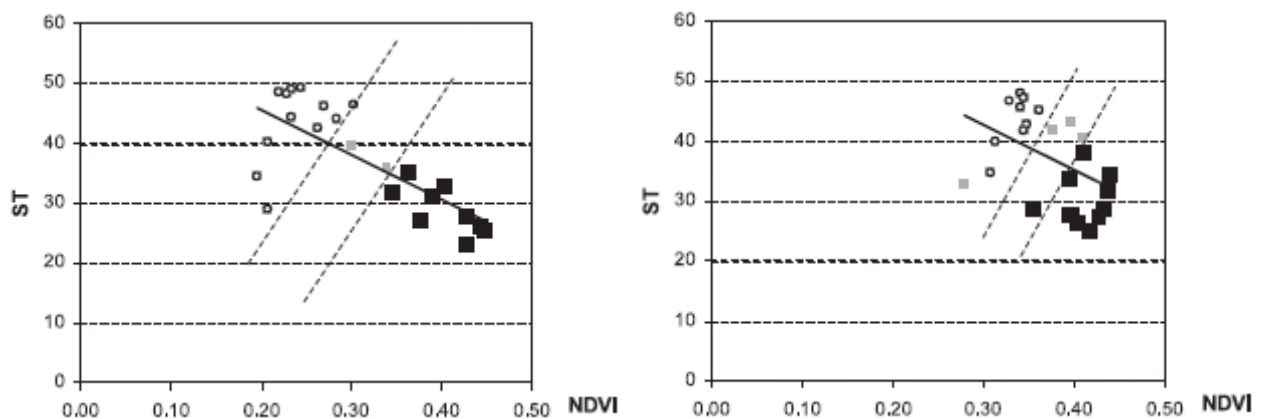


**Figure 3-8: Relations between NDVI, ST and FMC (Chuvienco et al., 2004) for grasslands (left) and shrublands (right). Black boxes refer to FMC>100% in grasslands and >110% for shrublands; white boxes refer to FMC<35% in grasslands and <80% for the shrublands; and grey boxes, the intermediate values. Solid lines show the regression of NDVI and ST. Dotted lines represent ranges of FMC in the inverse relation of NDVI and ST.**

Thermal infrared remote sensing has also been used as a reliable tool for coal fire detection and monitoring. Cracknell and Mansor (1992) first used Landsat-5 TM and NOAA-9 AVHRR data and found that night-time LST data was useful to isolate the warm areas from the background.

Prakash et al. (1997) used the Landsat TM TIR and SWIR bands to identify surface and subsurface fires separately, based on the surface temperature difference. More recently, Gangopadhyay et al. (2005) demonstrated Landsat-5 thermal remote sensing image can reveal the surface temperature anomalies effectively for quantitative study of coal fire. But in some cases, inaccurate pixel integrated temperatures are expected because of mixing of high temperature events (coal fires) and the background, which is a major drawback of low resolution data.

Recently, some global burnt area products produced using satellite data have been available. For example, at the global scale, ATSR-2 has been used with some success to map burned areas for the year 2000 (Kempeneers et al., 2002; Simon et al., 2004) through a project called GLOBSCAR initiated by ESA. The Global Burnt Area (GBA) product derived from SPOT VEGETATION (GBA-2000) provides monthly estimates, at 1km resolution for the year 2000 (Grégoire et al., 2003; Tansey et al., 2002; Tansey et al., 2004).

The ATSR-2 instrument day-time imagery was chosen for the GLOBSCAR project for a number of reasons (Simon et al., 2004):

- (i) near-infrared (NIR; 0.865 microns) and thermal infrared (TIR; 10.9 microns) channels are available on ATSR-2, both at high spectral resolution. These are the most useful spectral bands for global burnt area detection. The presence of a TIR is a particularly valuable asset compared to other optical sensors such as SPOT-VEGETATION;
- (ii) the day-time overpass of 10:30 at the equator is appropriate since at this time the ground already shows its characteristics in terms of heat exchange, but the information of clouds owing to the water surface evaporation is still limited. However, Mota et al. (2006) screened the algorithm 2 (308 K threshold) ESA World Fire Atlas (WFA), for the period 1997 - 2002, using night-time ATSR-2 3.7 $\mu$ m channel data, which is highly sensitive to radiation emitted at temperatures from 500K to 1000K. Use of night-time data is meant to minimise false alarms due to sun-glint, reflection off cloud edges, and bright soil surfaces. It is also expected to reduce false alarms caused by hot ground surfaces. Known limitations of the WFA are the inclusion of warm surfaces, gas flares, and city lights, and an underestimation of actual global fire activity, due to the time of satellite overpass. There is a potential to transfer the ATSR-2 fire detection and burnt area mapping to the AATSR, therefore, a long term fire observation record can be available for science community.

Huang and Siegert (2004) investigated the extent and impact of the forest and peatland fires in Central Kalimantan, Indonesia in 2002 using ENVISAT multisensor data. Reduced spatial resolution MERIS imagery was used to identify simple land cover features and smoke plumes. Fire hotspots were detected by using the 3.7 $\mu$ m channel of AATSR night-time acquisitions,

and burnt areas were detected by ASAR wide swath radar imagery acquired before and after the fire event. The capability of ENVISAT to acquire data from different sensors simultaneously or within a short period of time greatly enhances the possibilities to monitor fire occurrence and assess fire impact.

These global burned area products would be beneficial for some global change studies, such as atmospheric composition and chemistry, climate, biogeochemical cycling of nitrogen and carbon, hydrological cycle and stability of ecosystems. Whether the satellite LST combined with reflectance data could help to improve or validate the global burned area products needs further study. Moreover, there is an increasing interest in the biomass burning aerosol sources (Generoso, et al., 2003) and other gas emissions (e.g., CO<sub>2</sub>, CO and CH<sub>4</sub>), as well as the impact on tropospheric chemistry (Duncan et al., 2003). The total gases emission caused by biomass burning can be estimated using the combined the thermal sensors for burnt area mapping and other sensors for gas traces (e.g., GOME, SCIAMACHY and MIPAS).

### 3.5 Volcanic activity and earthquakes

Infrared radiance data from Earth-orbiting satellites have long been suggested as a suitable data source for documenting remote effusive volcanic activity (Mouginis-Mark et al., 1991; Rothery et al., 1988). Compared with AVHRR, ATSR has a shortwave infrared waveband at 1.6 $\mu$ m, which is close to the wavelength of peak spectral radiant emittance for surfaces at magmatic and near magmatic temperatures (~1000°C), making it useful for thermal studies of active lava. Wooster and Rothery (1997) studied the 1995 eruption of Fernandina Volcano using a time-series ATSR night-time dataset. The estimate of lava flow in the 1995 eruption of Fernandina using ATSR images is similar in magnitude to previous studies. The authors also concluded that their method could be transferred to the AATSR and MODIS sensors.

Some studies (e.g., Ouzounov and Freund, 2004; Tronin et al., 2004) show that thermal anomalies of LST are related to earthquakes and pre-seismic activities. Ouzounov and Freund (2004) analyzed mid-infrared emission prior to strong earthquakes using MODIS LST, SST and infrared emissivity data. They concluded that an anomalous LST of 3-4°C has been observed in the case study of Bhuj, Gujarat, India earthquake (magnitude = 7.7), consistent with similar reports from around the world. The rapid time-dependent evolution of the "thermal anomaly" makes it plausible that it is caused by changing mid-IR emissivity from the ground. Likewise anomalously low SST prior to a Bougainville Isle (magnitude = 7.2) seaquake, due to cold water upwelling, may have been caused by energy deposited into the ocean floor by the same physical process that leads to pre-earthquake "thermal anomalies" on land.

### 3.6 Forest mapping

AVHRR and MODIS data have also been used widely for land cover mapping. The growing demand for forest and soil mapping at both global and regional scales are emphasized in an European Commission report on a European-wide strategy, and a soil strategy for England. Some studies reported that NDVI data could not provide sufficient information for land cover mapping due to the influence of temperature, soil moisture and soil physical properties (Dobos et al., 2000; Dobos et al., 2001; Yang et al., 1997). Vegetation indices containing data acquired in the middle- and thermal-infrared channels performed better than the widely used NDVI (Foody, et al., 1996). Ehrlich et al. (1994) reported that thermal bands were useful for land cover discrimination, especially in tropical rainforest. The AATSR sensor includes seven spectral channels, with radiometric accuracy  $<0.1K$  that could be used for land cover mapping on its own or combined with MERIS data.

### 3.7 Energy balance (sensible/latent heat and evaporation)

LST plays an important role in the energy balance of the Earth. It is a major factor in determining the partition of the available energy into sensible and latent heat fluxes and also in determining the evaporation rate. The energy balance is based on:

$$R_n = (1 - \alpha)Q + L_{\downarrow} - L_{\uparrow} \quad (9)$$

$$R_n = (1 - \alpha)Q + \varepsilon\sigma(\varepsilon_a T_a^4 - T_s^4) \quad (10)$$

where  $R_n$  is net radiation,  $G$  is soil heat flux,  $Q$  is solar short-wave radiation,  $L_{\downarrow}$  is downwelling long-wave radiation from the atmosphere,  $L_{\uparrow}$  is upward long-wave radiation from the surface,  $T_s$  is radiometric surface temperature,  $T_a$  is air temperature,  $\alpha$  is spectral surface albedo,  $\varepsilon$  is surface emissivity,  $\sigma$  is the Stefan–Boltzmann constant, and  $\varepsilon_a$  is effective atmospheric emissivity (Brutsaert 1975).

Xue Y, et al. (1997) have developed a model to obtain the short-wave irradiation, long-wave radiation, latent heat flux and sensible heat flux at Earth's surface from the ATSR-1 thermal band data and the ATSR-2 visible and thermal band data. A technique for the derivation of LST and land surface emissivity retrieval using ATSR data has been proposed. The visible and near-infrared reflectances were derived from ATSR-2 visible spectral bands by using an atmospheric radiative transfer model developed previously. The models have been applied to the regional ATSR-2 data in the UK and global scale ATSR data in areas of open sea. The ATSR-2 data sets have been shown to be useful in helping the study of the large space heat flux exchange.

Using Landsat TM/ETM+ data and ground-based data, Zhang et al. (2006) constructed an integrated algorithm for estimating regional surface latent heat flux and daily evapotranspiration. Based on the surface energy balance system (SEBS), Jia et al. (2003) calculated the sensible heat flux from the ATSR imagery. A parameterization of the aerodynamic resistance for heat transfer (in term of  $\text{KB}^{-1}$ ) was applied for the first time at large spatial scales. For such large area analyses, SEBS requires wind speed, potential temperature and humidity of air at an appropriate reference height. The latter was taken as being the height of the planetary boundary layer (PBL) and the data used were fields generated by an advanced numerical weather prediction model, i.e. regional atmospheric climate model (RACMO), integrated over the PBL.

Bisht et al. (2005) estimated the net radiation over large heterogeneous areas for clear sky days using Terra MODIS data products including LST, land surface emissivity, surface albedo data, air temperature and air emissivity data. They explored a sinusoidal model which is capable of retrieving the diurnal variations of net radiation with a single instantaneous net radiation estimate from the satellite. The results using data over the Southern Great Plains had shown good agreement with ground-based observations.

### 3.8 Connection between convection and LST

Convective Available Potential Energy (CAPE) is a measure of the amount of energy available for convection. CAPE is directly related to the maximum potential vertical speed within an updraft; thus, higher values indicate greater potential for severe weather.

$$\text{CAPE} = \int_{p_n}^{p_f} (\alpha_p - \alpha_e) d_p \quad (11)$$

where  $\alpha_e$  is the environmental specific volume profile,  $\alpha_p$  is the specific volume of a parcel of air moving upward moist-adiabatically from the level of free convection,  $p_f$  is the pressure at the level of free convection, and  $p_n$  is the pressure at the level of neutral buoyancy. The value depends on whether the moist-adiabatic process is considered reversible or irreversible (conventionally irreversible) and whether the latent heat of freezing is considered (conventionally not).

López et al. (2001) found there is a linear relationship between the CAPE and the potential temperature for hail days which corresponds to the highest correlation between these two variables (see

Figure 3-9). The atmospheric instability increases with temperature, thus hails and storms are more likely to occur. The remotely sensed LST products combined with meteorological and atmospheric data have a potential to identify the areas of atmospheric instability.

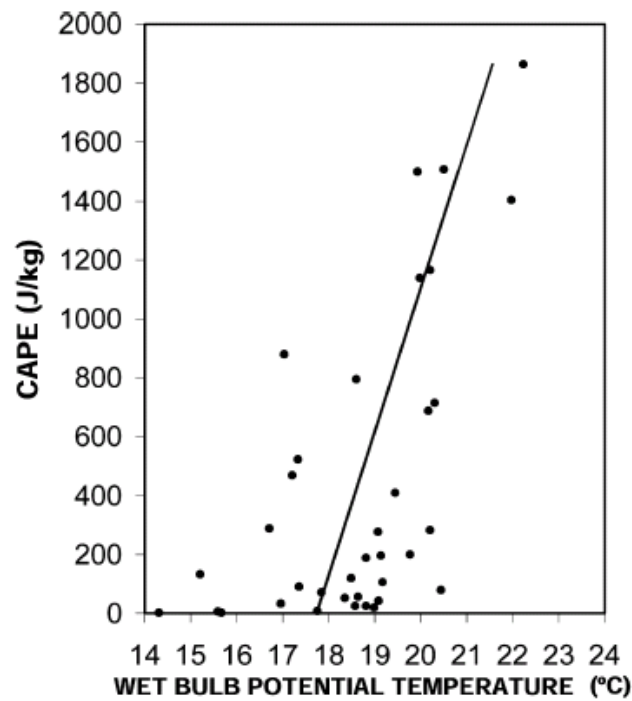


Figure 3-9: Relationship between the CAPE and the wet bulb potential temperature.

### 3.9 Connection between gas emissions and LST

The LST also effects the emission of gases. For example, tropical rainforests are estimated to be a major source of volatile organic compounds (VOCs) into the atmosphere (Guenther et al., 1995). Biogenic VOC (BVOC) mixing ratios above tropical rainforests are usually dominated by isoprene, but monoterpenes and other BVOCs are also observed (Rinne et al., 2002). Both isoprene and monoterpene emissions depend on temperature and light (Guenther et al., 1995; Rinne et al., 2002).

Greenberg et al. (1999) reported that day-time biogenic emissions increase with temperature and light, but appear to be balanced by changes in entrainment and oxidation (see Figure 3-10). Rinne et al., 2002 studied the canopy scale emissions of isoprene and monoterpenes from Amazonian rainforest as measured by eddy covariance and eddy accumulation techniques. Their results demonstrate that isoprene flux correlated with a light- and temperature-dependent emission activity factor, and even better with measured sensible heat flux. And also, the light and temperature dependence can have a significant effect on the modelled diurnal cycle of monoterpene emission as well as on the total monoterpene emission

(see Figure 3-11). Guenther et al. (1991) reported that terpene emissions from conifers demonstrate an exponential increase with increasing temperature.

VOC emissions have been estimated at the regional and global scales (Stewart et al., 2003; Guenther et al., 1995; Guenther et al., 2006). The controlling parameters for the VOC emissions are plant species, plant species distribution, biomass distribution, temperature, and light intensity. A Model of Emissions of Gases and Aerosols from Nature (MEGAN) has been used to quantify net terrestrial biosphere emission of isoprene into the atmosphere (Guenther et al., 2006). MEGAN is designed for both global and regional emission modelling and has global coverage with approximately 1km spatial resolution. The annual global emission estimated with MEGAN ranges from about 500 to 750Tg isoprene depending on the driving variables that are used. MEGAN driving variables (including temperature, solar radiation, Leaf Area Index (LAI), and plant functional type) are derived from models, satellite and ground observations (see Figure 3-12 and Figure 3-13). For this point of view, the land surface temperature together with land cover/LAI derived from satellite observations (e.g., AATSR LST product) would be useful in studying the global or regional VOC emissions. MEGAN isoprene emission estimates increase with increasing leaf temperature which is primarily driven by air temperature but is also influenced by solar radiation, humidity, wind speed and soil moisture.

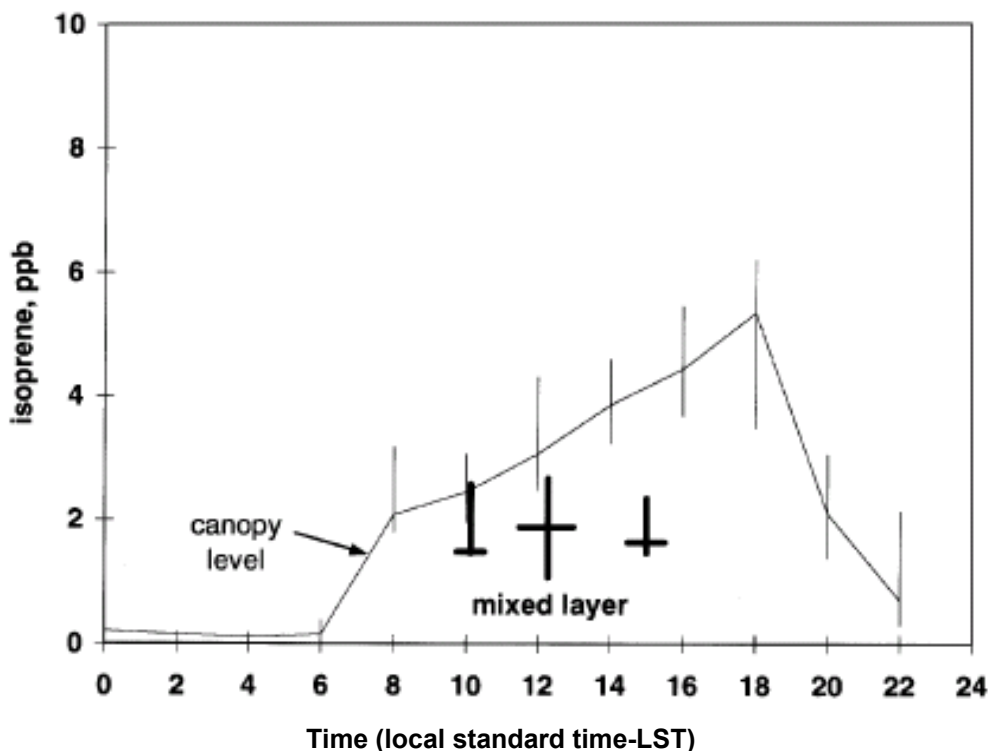


Figure 3-10: Comparison of isoprene concentrations at the canopy level and in the mixed layer from the Oak Ridge 1995 experiment. Canopy level concentrations

increased through late afternoon, while mixed layer concentrations remained fairly constant (Greenberg et al., 1999).

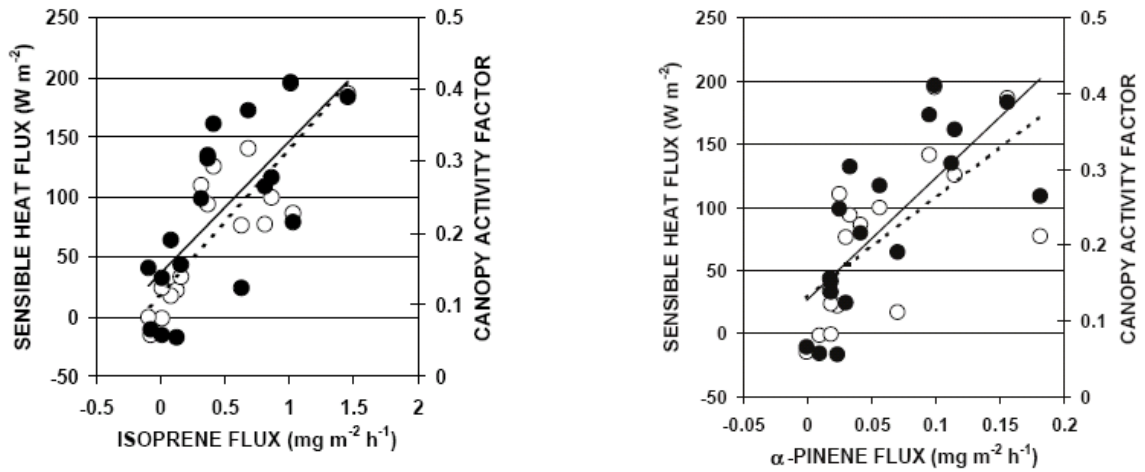


Figure 3-11: Isoprene and monoterpene ( $\alpha$ -pinene) emission. (a) Observed isoprene flux against temperature and light activity factor and sensible heat flux; (b) Observed fluxes of  $\alpha$ -pinene against temperature and light activity factor and sensible heat flux. (Note: solid circles and solid line describes temperature and light activity factor and open circles and dashed line describes sensible heat flux; Rinne et al., 2002)

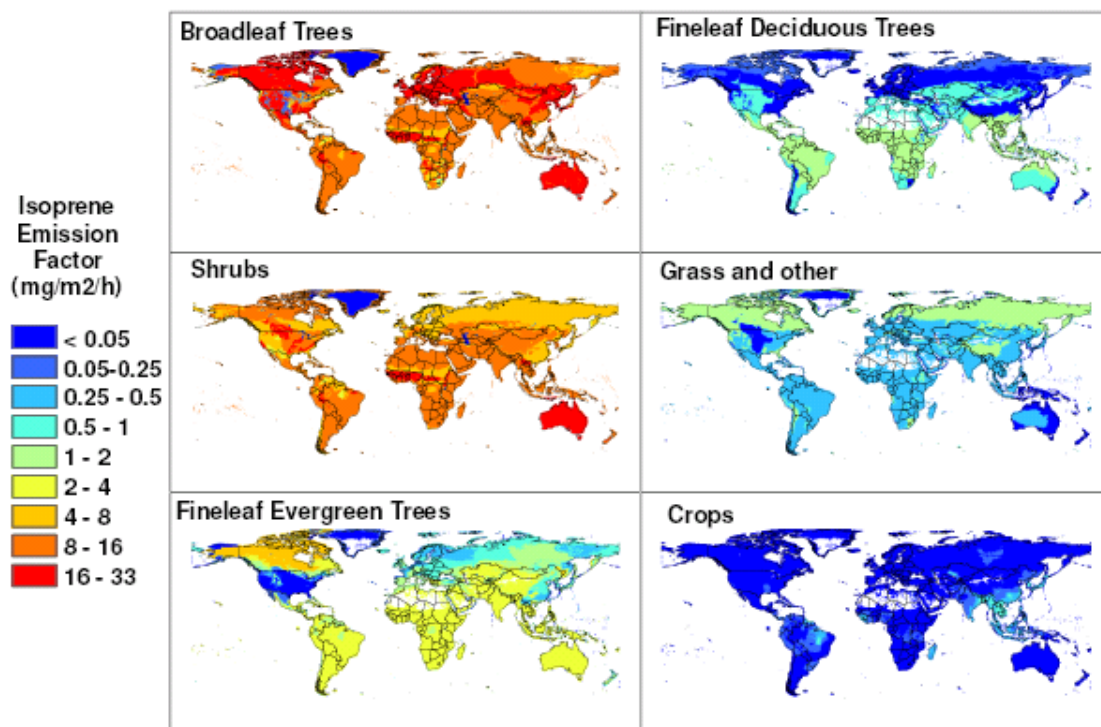


Figure 3-12: Global distribution of isoprene emission factors for the six MEGAN Plant Functional Types (PFTs). (Guenther et al., 2006)

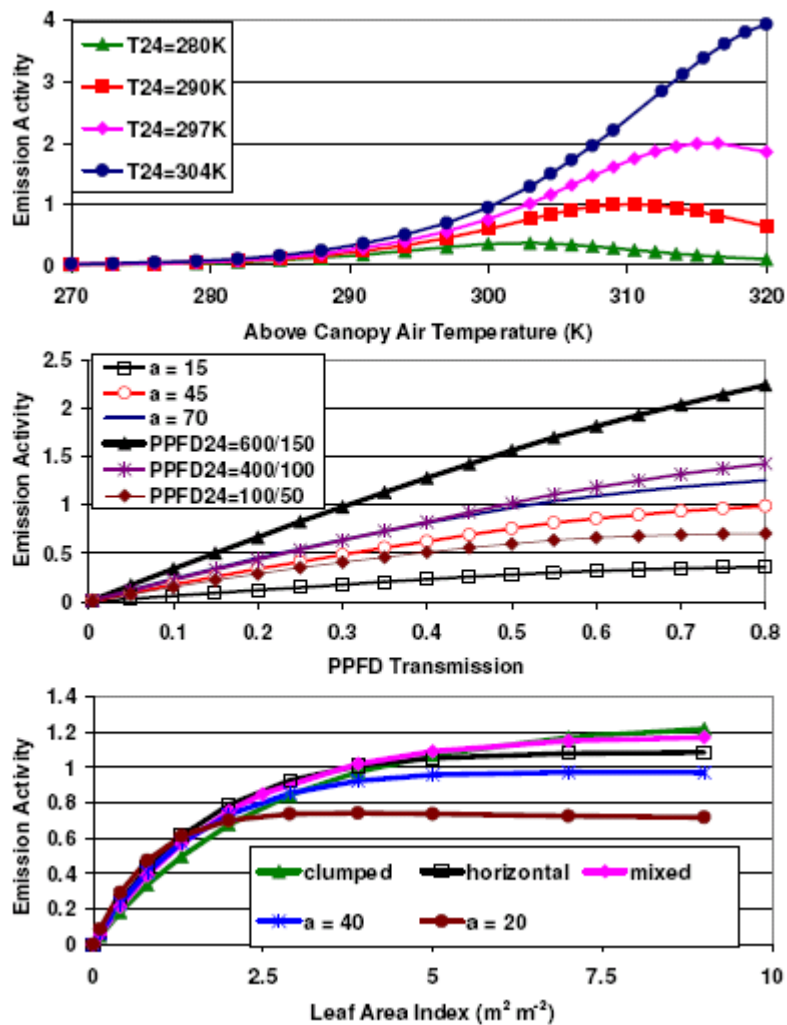


Figure 3-13: MEGAN estimates of isoprene emission response to current temperature (top), Photosynthetic Photon Flux Density (PPFD) transmission (middle) and LAI (bottom; Guenther et al., 2006).

### 3.10 Other applications

Prasad et al. (2006) used remotely sensed surface parameters to estimate crop yield over Iowa state, USA. Temporal annual average of NDVI, soil moisture, surface temperature and rainfall data for the period May to September have been used in the analysis for 19 years from 1982 to 2001. Results show that the model can be useful for forecasting crop yields such as corn and soybeans and other crops with acceptable accuracy.

Pepe et al. (2005) demonstrated snow cover monitoring in Alpine regions using ENVISAT MERIS and AATSR data. The AATSR 7 spectral bands across the range 0.55–12 mm include two spectral short-wave infrared bands where the reflectance of snow drops to near-zero while reflectance of most clouds remains high, allowing their discrimination, but its spatial resolution (1km) is not well suited for the study and remains a drawback for the use of this sensor.

### 3.11 Model predicted LST

The LST products calculated by the dynamic models have been used as an operational system in weather forecast and climate studies. For example, in the Met Office Surface Exchange Scheme (MOSES; Essery, et al., 2001), surface temperature  $T_*$  is interpreted as a surface skin temperature unless the canopy model is selected, in which case it is a canopy layer temperature for vegetated tiles. In the absence of snowmelt, the surface energy balance for each tile is

$$C_c \frac{dT_*}{dt} = R_N - H - LE - G_0, \quad (12)$$

$H$  and  $E$  are fluxes of sensible heat and moisture, and  $L$  is the latent heat of vaporization of snow-free tiles or sublimation for snow-covered or ice tiles. Where the surface net radiation is:

$$R_N = SW_N + LW_{\downarrow} - \sigma T_*^4, \quad (13)$$

$$SW_{Nj} = \sum_i (1 - \alpha_{ij}) SW_{\downarrow i} \quad (14)$$

$SW_{\downarrow}$  is the downward shortwave radiation and  $LW_{\downarrow}$  is the downward longwave radiation.

$SW_N$  is net all-band shortwave radiation on each tile.

MOSES has been integrated into the Met Office Unified Model (UM) and used for both weather forecast and climate predictions. The new generation model, upgraded from MOSES, is the Joint UK Land Environment Simulator (JULES) which provides a friendlier interface to integrate with satellite data. The European Centre for Medium-Range Weather Forecasts (ECMWF, 1995) has a numerical weather prediction (NWP) system, which cover the whole of Europea. LST products from these models can be compared with the remotely sensed LST products (Noyes, 2005). Comparisons of LST derived from satellite imagery with model estimations can provide a valuable insight into the performance of the current LST products and improve the accuracy of both satellite observations and model predictions. Recently the interests of model developers in integrating satellite observations into the model simulations are rising (Van den Hurk, et al., 2002). This synergy can take advantage of both satellite observations (spatial) and of model predictions (temporal).



## 4 POSSIBLE EXPLOITATION OF AATSR LST APPLICATIONS

Currently, the NOAA AVHRR and Terra/Aqua MODIS LST products are used in most applications of Earth observation due to their relatively longer dataset period and higher temporal resolution comparing with the AATSR LST. Although the AATSR LST data product has better accuracy than other currently available LST products, there are several limitations using this dataset in practise:

1. Compared with other infrared sensors, such as AVHRR, MODIS and SEVIRI, the temporal resolution of AATSR is relatively low (~3 days at the equator) and the day-time and night-time overpasses cannot be achieved on the same date in the most of the areas. Therefore, some applications using the difference between the day-time and night-time LST (e.g.,  $\Delta$ LST/NDVI and thermal inertia) cannot be used for the AATSR data. Whether the day-time LST/NDVI or 10 days/monthly average day-time and night-time LST data could be used in this application needs further investigation.
2. Literature already shows that the LST product retrieved from the satellite imagery can be used to detect the land surface changes, such as urbanization, deforestation and desertification. The AATSR LST product algorithm has been available since March 2004 and currently the LST products are available for ENVISAT back to 2002. However, this time series is not long enough for detecting land cover changes and for climate change studies. In comparison with AATSR, AVHRR has a relatively longer record (more than 20 years). Although there is a problem with the length of the AATSR LST record at the moment, it might be improved if the ENVISAT AATSR LST retrieval algorithm could be transferred to ERS-1 and ERS-2 ATSR data, and then 18 years continuous data would be available as for the (A)ATSR sea surface temperature (SST) data. This 18 year would be useful for detecting land surface changes and studying climate change.
3. Limitations such as cloud contamination might result in few images being available for some applications due to the relatively long revisit time, thus the research area should not be an often cloud-covered area. In addition, as the (A)ASTR was originally designed for monitoring SST, the signal could be saturated in some cases over land (e.g., desert or tropical area in the summer). Such areas should also be avoided.

Future studies could focus on one or two applications as follows:

- To explore whether the AATSR LST product can be used for urban heat island, deforestation and desertification studies. For example, the relationship between the LST/NDVI and land cover properties could be studied in a chosen location. Whether 10 days or monthly LST/NDVI could be used for some studies needs to be tested. The temporal trend of urban LST and land cover change may provide evidence for urban climate change.
- To explore the LST product in a water and energy balance study, including soil moisture, net radiation, sensible and latent heat flux. Soil moisture retrieval from satellite imagery can be still considered to be in an experimental stage, although there have been extensive efforts by the science community in the last 30 years. What are the advantages and disadvantages of thermal sensors compared with microwave sensors? What are the advantages/disadvantages of the energy balance derived from satellite data compared with an operational NWP system (e.g., MOSES, ECWMF)?
- To explore the use of (A)ATSR data for fire detection, burnt area mapping, pre-fire study (FMC) and the gas emissions due to biomass burning. What are the advantages and disadvantages of (A)ATSR compared with other sensors (SPOT-VEGETATION)? Can the LST product be combined with VIS and NIR reflectance to provide more valuable information than reflectance data alone? For estimation of gases emissions (CO<sub>2</sub>, CO, CH<sub>4</sub> and aerosols), whether combining with other sensors (SCIAMACHY, MIPAS) could be more useful? Given that the validation of the global fire products are still not available, whether the LST product (or combined with other data) can be useful for validation?
- A case study on the LST regional trend using long time period data to investigate any warming effect or to develop a model to predict future LST trends.
- To integrate the AATSR LST data into dynamic models (e.g., ECWMF, MOSES or JULES) and to investigate whether it can improve the model simulations. This needs a very accurate remotely sensed LST product.

## 5 REFERENCES

- Aires F., Prigent, C., and Rossow, W., 2004. Temporal interpolation of global surface skin temperature diurnal cycle over land under clear and cloudy conditions, *J. Geophys. Res.*, 109, D04313, doi:10.1029/2003JD003527.
- Barbosa, P.M., Grégoire, J-M. and Pereira, J.M.C., 1999. An algorithm for extracting burned areas from time series of AVHRR GAC data applied at a continental scale. *Remote Sensing of Environment*, 69(3): 253-263.
- Betts, R.A., 2001. Biogeophysical impacts of land use on present-day climate: near-surface temperature change and radiative forcing. *Atmospheric Science Letters*, 2(1-4): 39-51.
- Bisht, G., Venturini, V., Islam, S. and Jiang, L., 2005. Estimation of the net radiation using MODIS (Moderate Resolution Imaging Spectroradiometer) data for clear sky days. *Remote Sensing of Environment*, 97(1): 52-67.
- Brutsaert, W. H., 1975. On a derivable formula for long-wave radiation from clear skies. *Water Resources Research*, 11:742-744.
- Cabral, A., Vasconcelos, M.J.P.d., Pereira, J.M.C., Bartholome, J.E. and Mayaux, P., 2003. Multi-temporal compositing approaches for SPOT-4 vegetation. *International Journal of Remote Sensing*, 24(16): 3343-3350.
- Carlson, T.N. and Arthur, S.T., 2000. The impact of land use - land cover changes due to urbanization on surface microclimate and hydrology: a satellite perspective. *Global Planet, Change* 25: 49-65.
- Chladil, M.A. and Nunez, M., 1995. Assessing grassland moisture and biomass in Tasmania. The application of remote sensing and empirical models for a cloudy environment. *International Journal of Wildland Fire*, 5: 165-171.
- Chuvieco, E., Cocero, D., Riano, D., Martin, P., Martinez-Vega, J., de la Riva, J., Perez, F., 2004. Combining NDVI and surface temperature for the estimation of live fuel moisture content in forest fire danger rating. *Remote Sensing of Environment*, 92(3): 322-331.
- Chuvieco, E., Deshayes, M., Stach, N., Cocero, D. and Riano, D., 1999. Short-term fire risk: Foliage moisture content estimation from satellite data. In E. Chuvieco (Ed.), *Remote sensing of large wildfires in the European Mediterranean Basin.*, Berlin: Springer-verlag.
- Chuvieco, E., Ventura, G., Martin, M.P. and Gomez, I., 2005. Assessment of multitemporal compositing techniques of MODIS and AVHRR images for burned land mapping. *Remote Sensing of Environment*, 94(4): 450-462.
- Climate change, 2001. The Scientific Basis. Contribution of Working Group I to the Third Assessment Report of the Intergovernmental Panel on Climate Change (Houghton, J.T., et al., eds). Cambridge University Press.
- Cracknell, A.P., Mansor, S.B., 1992. Detection off sub-surface coal fires using Landsat Thematic Mapper data. *Int. Arch. Photogram. Rem. Sens*, 29(b7), 750-753.
- Dimitrakopoulos, A. and Papaioannou, K.K., 2001. Flammability assessment of Mediterranean forest fuels. *Fire Technology*, 37: 143-152.
- Dobos, E., Micheli, E., Baumgardner, M.F., Biehl, L. and Helt T., 2000. Use of combined digital elevation model and satellite radiometric data for regional soil mapping. *Geoderma*, 97(3-4):367-391.
- Dobos, E., Montanarella, L., Nègre, T. and Micheli E., 2001. A regional scale soil mapping approach using integrated AVHRR and DEM data. *International Journal of Applied Earth Observation and Geoinformation*, 3 (1): 30-42.

- Dousset, B. and Gourmelon, F., 2003. Satellite multi-sensor data analysis of urban surface temperatures and landcover. *ISPRS Journal of Photogrammetry and Remote Sensing, Algorithms and Techniques for Multi-Source Data Fusion in Urban Areas*, 58(1-2): 43-54.
- Duncan B.N., Bey I., Chin M., Mickley L.J., Fairlie T.D., Martin R.V. and Matsueda H., 2003. Indonesian wildfires of 1997: Impact on tropospheric chemistry. *J GEOPHYS RES-ATMOS* 108 (D15).
- ECMWF, 1995. The description of the ECMWF/WCRP level III-A global atmospheric data archive.
- Ehrlich, D., Estes, J.E. and Singh, A., 1994. Applications of NOAA-AVHRR 1km data for environmental monitoring. *International Journal of Remote Sensing* 15: 145-161.
- ESA, 2002. The AATSR Products User Guide.
- Essery, R., Best, M. and Cox, P.M., 2001. MOSES 2.2 Technical Documentation. Hadley Centre technical note 30. Met Office, UK.
- Foody, G.M., Boyd, D.S. and Curran, P.J., 1996. Relations between tropical forest biophysical properties and data acquired in AVHRR channels 1-5. *International Journal of Remote Sensing* 17: 1314-1355.
- Fraser, R.H., Li, Z. and Cihlar, J., 2000. Hotspot and NDVI Differencing Synergy (HANDS): A New Technique for Burned Area Mapping over Boreal Forest. *Remote Sensing of Environment*, 74(3): 362-376.
- Gallo, K.P., McNab, A.L., Karl, T.R., Brown, J.F., Hood, J.J., Tarpley, J.D., 1993. The use of a vegetation index for assessment of the urban heat island effect. *International Journal of Remote Sensing*. 14(11): 2223-2230.
- Gangopadhyay, P.K., Lahiri-Dutt, K. and Saha K., 2005. Application of remote sensing to identify coalfires in the Raniganj Coalbelt, India. *International Journal of Applied Earth Observation and Geoinformation*, JAG-117.
- Generoso S., Breon F.M., Balkanski Y., Boucher O. and Schulz M., 2003. Improving the seasonal cycle and interannual variations of biomass burning aerosol sources. *ATMOS CHEM PHYS* 3: 1211-1222 AUG 22 2003.
- Gillies, R.R., Carlson, T.N., Cui, J., Kustas, W.P. and Humes, K.S., 1997. A verification of the 'triangle' method for obtaining surface soil water content and energy fluxes from remote measurements of the Normalized Difference Vegetation Index (NDVI) and surface radiant temperature. *International Journal of Remote Sensing*, 18(15): 3145-3166.
- Greenberg, J. P., Guenther, A., Zimmerman, P., Baugh, W., Geron, C., Davis, K., Helmig D. and Klinger, L. F., 1999. Tethered balloon measurements of biogenic VOCs in the atmospheric boundary layer. *Atmospheric Environment*, 33(6): 855-867
- Grégoire, J-M., Tansey, K., Silva, J.M.N., 2003. The GBA2000 initiative: Developing a global burned area database from SPOT-VEGETATION imagery. *International Journal of Remote Sensing*, 24(6), 1369-1376.
- Guenther, A., R. Monson, and R. Fall, 1991. Isoprene and monoterperene emission rate variability: observations with eucalyptus and emission rate algorithm development, *J. Geophys. Res.* 96 (D6), 10799-10808.
- Guenther, A., Hewitt, C.N., Erickson, D., Fall, R., Geron, C., Graedel, T., Harley, P., Klinger, L., Lerdau, M., McKay, W.A., Pierce, T., Scholes, B., Steinbrecher, R., Tallamraju, R., Taylor, J., Zimmerman, P., 1995. A global model of natural volatile organic compound emissions. *Journal of Geophysical Research* 100, 8873-8892.
- Guenther, A., Karl, T., Harley, P., Wiedinmyer, C., Palmer, P.I. and Geron C., 2006. Estimates of global terrestrial isoprene emissions using MEGAN (Model of Emissions of Gases and Aerosols from Nature) *Atmospheric Chemistry and Physics Discussions* 6:107-173.

- Houghton, J. T., Meira filho, L. G., Bruce, J., Lee, H., Callander, B. A., Haites, E., Harris, N., and Maskell, K., 1995, *Climate Change 1994: Radiative Forcing of Climate Change* (Cambridge: Cambridge University Press).
- Huang, S. and Siegert, F., 2004. ENVISAT multisensor data for fire monitoring and impact assessment. *International Journal of Remote Sensing*, 25(20): 4411-4416.
- Hung, T., Uchihama, D., Ochi, S. and Yasuoka, Y., 2006. Assessment with satellite data of the urban heat island effects in Asian mega cities. *International Journal of Applied Earth Observation and Geoinformation*, 8(1): 34-48.
- Jia, L., Su, Z.B., van den Hurk, B., Menenti M., Moene A., De Bruin H.A.R., Yrisarry J.J.B., Ibanez M., Cuesta A., 2003. Estimation of sensible heat flux using the Surface Energy Balance System (SEBS) and ATSR measurements. *PHYS CHEM EARTH* 28 (1-3): 75-88.
- Jin, M. and Dickinson R. E., 1999. Interpolation of surface radiative temperature measured from polar orbiting satellites to a diurnal cycle 1. Without clouds, *J. Geophys. Res.*, 104(D2), 2105-2116, 10.1029/1998JD200005.
- Kempeneers, P., Swinnen, E. and Fierens F., 2002. GLOBSCAR final report. VITO TAP/N7904/FF/FR-001 version 1.2, European Space Agency, Paris.
- Kerr, Y.H., Lagouarde, J.P. and Imbernon, J., 1992. Accurate land surface temperature retrieval from AVHRR data with use of an improved split window algorithm. *Remote Sensing of Environment*, 41(2-3): 197-209.
- Kustas, W.P. and Norman, J.M., 1996. Use of remote sensing for evapo-transpiration monitoring over land surfaces. *Hydrological Sciences Journal*, 41(495-516).
- Lambin, E.F. and Ehrlich, D., 1997. Land-cover changes in sub-saharan Africa (1982-1991): Application of a change index based on remotely sensed surface temperature and vegetation indices at a continental scale. *Remote Sensing of Environment*, 61(2): 181-200.
- Li, F. Jackson, T.J., Kustas, W.P., Schmugge, T.J., French, A.N., Cosh, M.H. and Bindlish, R., 2004. Deriving land surface temperature from Landsat 5 and 7 during SMEX02/SMACEX. *Remote Sensing of Environment, Soil Moisture Experiment (SMEX02)*, 92(4): 521-534.
- Lillesand, T.M. and Kiefer, R.W., 1987. *Remote sensing and image interpretation*. Wiley, New York.
- Llewellyn-Jones, D. Edwards, M. C., Mutlow, C. T., Birks, A. R., Barton, I. J., Tait, H., 2001. AATSR: Global-Change and Surface-Temperature Measurements from Envisat, ESA bulletin February 2001. 105, 11–21.
- López, L., Marcos, J.L., Sánchez, J.L., Castro, A., and Fraile, R., 2001. CAPE values and hailstorms on northwestern Spain. *Atmospheric Research*, 56(1-4): 147-160.
- Manzo-Delgado, L., Sanchez-Colon, S. and Alvarez, R., 2005. Multitemporal analysis of NDVI and land surface temperature for modeling the probability of forest fire occurrence in central Mexico, 2005 International Workshop on the Analysis on Multi-Temporal Remote Sensing Images, pp. 177-181.
- Meyer, W.B., 1996. *Human Impact on the Earth*. Cambridge University Press, Cambridge.
- Mitra, D.S. and Majumdar, T.J., 2004. Thermal inertia mapping over the Brahmaputra basin, India using NOAA-AVHRR data and its possible geological applications. *International Journal of Remote Sensing*, 225(16): 3245-3260.
- Mota BW, Pereira JMC, Oom D, Vasconcelos MJP and Schultz M, 2006. Screening the ESA ATSR-2 World Fire Atlas (1997-2002). *Atmospheric Chemistry and Physics* 6: 1409-1424.
- Mougini-Mark, P. Rowland, S., Francis, P., Friedman, T., Garbeil, H., Gradie, J., Self, S., Wilson, L., Crisp, J., Glaze, L., Jones, K. and Kahle, A., 1991. Analysis of active volcanoes from the earth observing system. *Remote Sensing of Environment*, 36(1): 1-12.



- Noyes, E.J., 2005. Technical Assistance for the Validation of AATSR Land Surface Temperature Products. Task 2 Report – November 2005. Contract Number: 19054/05/NL/FF.
- Noyes, E.J., 2006. An investigation into the accuracy of surface temperature retrievals from the AATSR. PhD Thesis, University of Leicester, UK, 1-17 pp.
- Noyes, E.J., Soria, G., Sobrino, J.A., Remedios, J.J., Llewellyn-Jones, D.T., Corlett, G.K., in press. AATSR land surface temperature product algorithm verification over a WATERMED site. *Advances in Space Research*, In Press, Corrected Proof.
- Ottele, C. and Vidal-Madjar, D., 1992. Estimation of land surface temperature with NOAA9 data. *Remote Sensing of Environment*, 40(1): 27-41.
- Ouzounov, D. and Freund, F., 2004. Mid-infrared emission prior to strong earthquakes analyzed by remote sensing data. *Advances in Space Research*, 33(3): 268-273.
- Owen, T.W., Carlson, T.N. and Gillies, R.R., 1998. An assessment of satellite remotely sensed land cover parameters in quantitatively describing the climate effect of urbanization. *International Journal of Remote Sensing*, 19(9): 1663-1681.
- Paltridge, G.W. and Barber, J., 1988. Monitoring grassland dryness and fire potential in Australia with NOAA/AVHRR data. *Remote Sensing of Environment*, 25(3): 381-394.
- Pepe, M., Brivio, P.A., Rampini, A., Rota, F. and Boschetti, M., 2005. Snow cover monitoring in Alpine regions using ENVISAT optical data. *INT J REMOTE SENS* 26 (21): 4661-4667.
- Pongrácz, R., Bartholy, J., Dezső, Zs., 2006: Remotely sensed thermal information applied to urban climate analysis. *Advances in Space Research*, 37, 2191-2196. DOI: 10.1016/j.asr.
- Prakash, A. 2000. Thermal remote sensing: concepts, issues and applications. *International Archives of Photogrammetry and Remote Sensing*. Vol. XXXIII, part B1. Amsterdam, 2000.
- Prakash, A., Gupta, R.P., Saraf, A.K., 1997. A Landsat TM based comparative study of surface and subsurface fires in the Jharia coalfield, India. *International Journal of Remote Sensing*, 18(11), 2463-2469.
- Prasad, A.K., Chai, L., Singh, R.P., and Kafatos, M., 2006. Crop yield estimation model for Iowa using remote sensing and surface parameters. *Applied Earth Observation and Geoinformation*, 8: 26-33.
- Prata, A.J., 2000. Land surface temperature measurement from space: AATSR Algorithm Theoretical Basis Document. ESA/CSIRO publication.
- Prata, A.J. and Cecket, R.P., 1999. An assessment of the accuracy of land surface temperature determination from the GMS-5 VISSR. *Remote Sensing of Environment*, 67(1): 1-14.
- Qin, Z. and Karnieli, A., 1999. Progress in the remote sensing of land surface temperature and ground emissivity using NOAA-AVHRR data. *International Journal of Remote Sensing*, 20(12): 2367-2393.
- Reutter, H., Olesen, F.-S. and Fischer, H., 1996. Determination of Land Surface Temperatures from AVHRR and METEOSAT Data. Environment, final report, Insitut f'ur Meteorologie und Klimaforschung.
- Rinne, H.J.I., Guenther, A.B., Greenberg, J.P., Harley, P.C., 2002. Isoprene and monoterpene fluxes measured above Amazonian rainforest and their dependence on light and temperature *Atmospheric Environment* 36 (14): 2421-2426.
- Rothery, D.A., Francis, P.W. and Wood, C.A., 1988. Volcano monitoring using short wavelength infrared data from satellites. *Journal of Geophysical Research*, 93: 7993-8008.
- Savtchenko, A. Ouzounov, D., Ahmad, S., Acker, J., Leptoukh, G., Kozianna, J. and Nickless, D., 2004. Terra and Aqua MODIS products available from NASA GES DAAC. *Advances in Space Research. Trace Constituents in the Troposphere and Lower Stratosphere*, 34(4): 710-714.



- Simard, A.J., 1968. The moisture content of forest fuels - A review of the basic concepts. Information report FF-X-14., Forest Fire Research Institute, Ottawa, Ontario.
- Simon, M., Plummer, S., Fierens, F., Hoelzemann J.J. and Arino O., 2004. Burnt area detection at global scale using ATSR-2: The GLOBSCAR products and their qualification, *Journal of Geophysics Research*, 109, doi: 10.1029/2003JD003622, in press.
- Sobrino, J.A. and Raissouni, N., 2000. Toward remote sensing methods for land cover dynamic monitoring: application to Morocco. *International Journal of Remote Sensing*, 21(2): 353-366.
- Sousa, A.M.O., Pereira, J.M.C. and Silva, J.M.N., 2003. Evaluating the performance of multitemporal image compositing algorithms for burned area analysis. *International Journal of Remote Sensing*, 24(6): 1219-1236.
- Stewart, H. E., C. N. Hewitt, R. G. H. Bunce, R. Steinbrecher, G. Smiatek, and T. Schoenemeyer, 2003. A highly spatially and temporally resolved inventory for biogenic isoprene and monoterpene emissions: Model description and application to Great Britain, *J. Geophys. Res.*, 108(D20), 4644, doi:10.1029/2002JD002694.
- Tansey, K., 2002. Implementation of regional burnt area algorithms for the GBA2000 initiative, Rep. EUR20532, 159pp., Eur.Comm., Luxembourg.
- Tansey, K., Grégoire J-M., Stroppiana, D., Sousa, A., Silva, J., Pereira, J.M.C., Boschetti, L., Maggi, M., Brivio, P.A., Fraser, R., Flasse, S., Ershov, D., Binaghi, E., Graetz, D. and Peduzzi, P., 2004. Vegetation burning in the year 2000: Global burned area estimates from SPOT VEGETATION data. *Journal of Geophysical Research-Atmospheres*, 109, D14S03, doi:10.1029/2003JD003598.
- Tramutoli, V., Claps, P., Marella, M., Pergola, N. and Sileo, C., 2000. Feasibility of hydrological application of thermal inertia from remote sensing, 2nd Plinius Conference on Mediterranean Storms., Siena, Italy.
- Tronin, A.A., Biagi, P.F., Molchanov, O.A., Khatkevich, Y.M. and Gordeev, E.I., 2004. Temperature variations related to earthquakes from simultaneous observation at the ground stations and by satellites in Kamchatka area. *Physics and Chemistry of the Earth, Parts A/B/C*, 29(4-9): 501-506.
- Van den Hurk, B.J.J.M., Jia, L., Jacobs, C., Menenti M., Li Z.L., 2002. Assimilation of land surface temperature data from ATSR in an NWP environment - a case study. *International Journal of Remote Sensing*, 23(24): 5193-5209.
- Verstraeten, W.W., Veroustraete, F., van der Sande, C.J., Grootaers, I. and Feyen, J., 2006. Soil moisture retrieval using thermal inertia, determined with visible and thermal spaceborne data, validated for European forests. *Remote Sensing of Environment*, 101(3): 299-314.
- Wan, Z., 1999. MODIS land-surface temperature algorithm theoretical basis document, Version 3.3. NASA Documents. Website [http://modis.gsfc.nasa.gov/atbd/atbd\\_mod11.pdf](http://modis.gsfc.nasa.gov/atbd/atbd_mod11.pdf).
- Wooster, M.J. and Rothery, D.A., 1997. Time-series analysis of effusive volcanic activity using the ERS along track scanning radiometer: The 1995 eruption of Fernandina volcano, Galapagos Islands. *Remote Sensing of Environment*, 62(1): 109-117.
- Xue Y., Lawrence S.P. and Llewellyn-Jones D.T., 1997. Use of ATSR data to estimate surface fluxes over land and sea. Third ERS symposium on space at the service of our environment, ESA special publications, vols. ii & iii 414: 791-794.
- Yang, W., Yang, L. and Merchant J.W., 1997. An assessment of AVHRR/NDVI-ecoclimatological relations in Nebraska, USA. *International Journal of Remote Sensing* 18: 2161-2180.
- Zhang, Y., Liu, C., Lei, Y., Tang, Y., Yu, Q., Shen, Y. and Sun, H., 2006. An integrated algorithm for estimating regional latent heat flux and daily evapotranspiration. *International Journal of Remote Sensing*, 27 (1): 129-152.



## APPENDIX A: LIST OF ACRONYMS

AATSR	Advanced Along-Track Scanning Radiometer
(A)ATSR	All three ATSR instruments
AEB	(A)ATSR Exploitation Board
AEP	(A)ATSR Exploitation Plan
ASAR	Advanced Synthetic Aperture Radar
ATI	Apparent Thermal Inertia
ATSR	Along-Track Scanning Radiometer
ATSR-1	The ATSR instrument on the ERS-1 satellite
ATSR-2	The ATSR instrument on the ERS-2 satellite
AVHRR	Advanced Very High Resolution Radiometer
BT	Brightness Temperature
BVOC	Biogenic Volatile Organic Compound
CAPE	Convective Available Potential Energy
ECMWF	European Centre for Medium Range Weather Forecasting
Envisat	Environmental Satellite
EO	Earth Observation
ERS	Earth Remote Sensing satellite
ESA	European Space Agency
fAPAR	<i>fraction</i> of Absorbed Photosynthetically Active Radiation
FMC	Fuel Moisture Content
GAC	Global Area Coverage
GBA	Global Burnt Area
GOME	Global Ozone Monitoring Experiment
JULES	Joint UK Land Environment Simulator
LAI	Leaf Area Index
LST	Land Surface Temperature
MEGAN	Model of Emissions of Gases and Aerosols from Nature
MERIS	Medium Resolution Imaging Spectrometer



MIPAS	Micholson Interferometer for Passive Atmospheric Sounding
MODIS	MODerate resolution Imaging Spectroradiometer
MOSES	Met Office Surface Exchange Scheme
NDVI	Normalised Difference Vegetation Index
NIR	Near Infra Red
NOAA	National Oceanic and Atmospheric Administration
NWP	Numerical Weather Prediction
PBL	Planetary Boundary Layer
PFT	Plant Functional Type
PI	Principal Investigator
PPFD	Photosynthetic Photon Flux Density
RACMO	Regional Atmospheric Climate MOdel
SCHIAMACHY	SCanning Imaging Absorption spectroMeter for Atmospheric Chartography
SEBS	Surface Energy Balance System
SEVIRI	Spinning Enhanced Infrared and Visible Imager
SMC	Soil Moisture Content
SMSI	Soil Moisture Saturation Index
SST	Sea Surface Temperature
ST	Surface Temperature
TI	Thermal Inertia
TIR	Thermal Infra Red
TM	(Landsat) Thematic Mapper
UHI	Urban Heat Island
UM	Unified Model
UTC	Coordinated Universal Time
VOC	Volatile Organic Compound
WFA	World Fire Atlas